

Magnetic ground state and exchange interactions in the Ising chain ferromagnet CoNb_2O_6

Subhash Thota ^{1,*}, Sayandeep Ghosh,¹ Maruthi R.,¹ Deep C. Joshi,¹ Rohit Medwal,²
Rajdeep S. Rawat,² and Mohindar S. Seehra ³

¹Department of Physics, Indian Institute of Technology, Guwahati, Assam 781039, India

²National Institute of Education, Nanyang Technological University Singapore, 637616 Singapore

³Department of Physics & Astronomy, West Virginia University, Morgantown, West Virginia 26506, USA



(Received 20 November 2020; accepted 25 January 2021; published 8 February 2021)

Reported here are measurements and analysis of the magnetization (M) versus temperature (1.9–400 K) in magnetic fields H up to 90 kOe for a polycrystalline sample of Ising chain ferromagnet CoNb_2O_6 with $T_C = 2.9$ K. For $T > T_C$, the fit of magnetic susceptibility $\chi = M/H$ ($H = 300$ Oe) to $\chi = \chi_0 + C/(T - \Theta)$ with $\chi_0 = 0.0009$ emu mol⁻¹ Oe⁻¹ determined from high- T data yields $\Theta = 11$ K and magnetic moment $\mu = 4.994 \mu_B$ per Co^{2+} ion calculated from experimental $C = 3.12$ emu K mol⁻¹ Oe⁻¹. Values of g obtained from $\mu^2/\mu_B^2 = g^2 S(S + 1)$ for spin $S = 1/2$ and $3/2$ are used to determine $\mu_Z = g S \mu_B$ and compared with μ_Z obtained from saturation magnetization and neutron diffraction for $T \ll T_C$. This analysis of the data for both above and below T_C shows that the ground state of Co^{2+} in CoNb_2O_6 has the effective spin $S = 1/2$ and not $S = 3/2$ expected from Hund's rules, the $S = 1/2$ ground state resulting from the combined effects of a noncubic crystalline field and spin-orbit coupling. The fit of the data for $T > T_C$ to $\chi = \chi_0 + (C/T) \exp(J_0/2k_B T)$ valid for an Ising chain with $S = 1/2$ yields the intrachain ferromagnetic exchange constant $J_0/k_B = 6.2$ K, whereas the g value with $S = 1/2$ and the experimental critical fields for spin flips yields interchain antiferromagnetic exchange constants $J_1/k_B = -0.42$ K and $J_2/k_B = -0.67$ K.

DOI: [10.1103/PhysRevB.103.064415](https://doi.org/10.1103/PhysRevB.103.064415)

I. INTRODUCTION

There has always been a great need to find real systems whose measured properties can be used to test the predictions of theoretically solvable models since such comparisons provide great insight into underlining physics. One such recent case is the predictions of excitations near a quantum critical point (QCP), which have been recently tested in the Ising ferromagnet CoNb_2O_6 when a critical field $H_C = 52.5$ kOe is applied transverse to the Ising axis [1–4]. Prior to these recent observations of quantum fluctuations well above $T = 0$ K in CoNb_2O_6 [2–5], magnetic properties of this highly anisotropic system have been reported by a number of groups since 1973 using magnetometry, neutron diffraction, and ⁹³Nb nuclear magnetic resonance, both in powder and single-crystal samples [6–17].

The first reports on the structural and magnetic properties of CoNb_2O_6 during the 1970s [6–8] showed that it crystallized in the columbite structure (space group $Pbcn$) with an orthorhombic unit cell of dimensions $a = 14.167$ Å, $b = 5.714$ Å, and $c = 5.048$ Å. In this structure, CoO_6 octahedra form chains along the c -axis with isosceles triangular geometry in the ab -plane. Magnetically, the Co^{2+} moments lie in the ac -plane with angle $\alpha \sim 31^\circ$ from the c -axis in a zigzag fashion due to the two crystallographically inequivalent sites. The ac magnetic susceptibility (χ_{ac}) studies of Scharf *et al.* [8] in single crystals showed a peak in χ_{ac} near $T = 3$ K along the a -axis and near 2 K along the c -axis with no anomaly along the b -axis. These results were confirmed later by

Hanawa *et al.* [9], who also measured the temperature dependence of the specific heat. The magnetic field dependence of the magnetization (M) at 1.4 K measured by Maartense *et al.* [7] for H parallel to the c -axis showed jumps in M near $H_{C1} \sim 300$ Oe and $H_{C2} \sim 3$ kOe leading to saturation magnetization $M_S \sim 14000$ emu mol⁻¹ for $H > H_{C2}$. Magnetic and neutron diffraction measurements for H parallel to the c -axis reported by Heid *et al.* [11] showed that for $H < H_{C1}$, the magnetic phase transition from the paramagnetic (PM) phase to sinusoidally amplitude-modulated incommensurate (IC) magnetic ordering occurs at $T_C = 2.95$ K followed by antiferromagnetic (AFM) ordering below $T_N = 1.97$ K. The IC magnetic phase is characterized by the propagation vector $Q = (0, q_y, 0)$ with temperature-dependent q lying in the range of $1/3 < q < 1/2$. Because of the isosceles triangular geometry in the ab plane, the AFM phase below T_N has degeneracy with phases of propagation vector $Q = (0, 0.5, 0)$ and $(0.5, \pm 0.5, 0)$ that was identified using neutron diffraction [12,14,15,17].

The rich details of the H - T phase diagram of CoNb_2O_6 for H along different axes have been investigated by a number of groups. Following up on the earlier studies in Refs. [7–11] mentioned above, the phase diagram for H parallel to the c -axis was later confirmed in more detail by Kobayashi *et al.* [12–14]. Kobayashi *et al.* [15] also presented the H - T phase diagram for H along the a -axis, whereas Liang *et al.* [3] have reported the phase diagram for H parallel to the b -axis using specific-heat measurements, which yielded $T_C = 2.85$ K for $H = 0$. These results on the H - T phase diagrams for H along the c - and b -axis are summarized in Fig. 1, a discussion of our results will be presented later. For H along the b -axis, T_C decreases with an increase in H , reaching QCP

*subhasht@iitg.ac.in

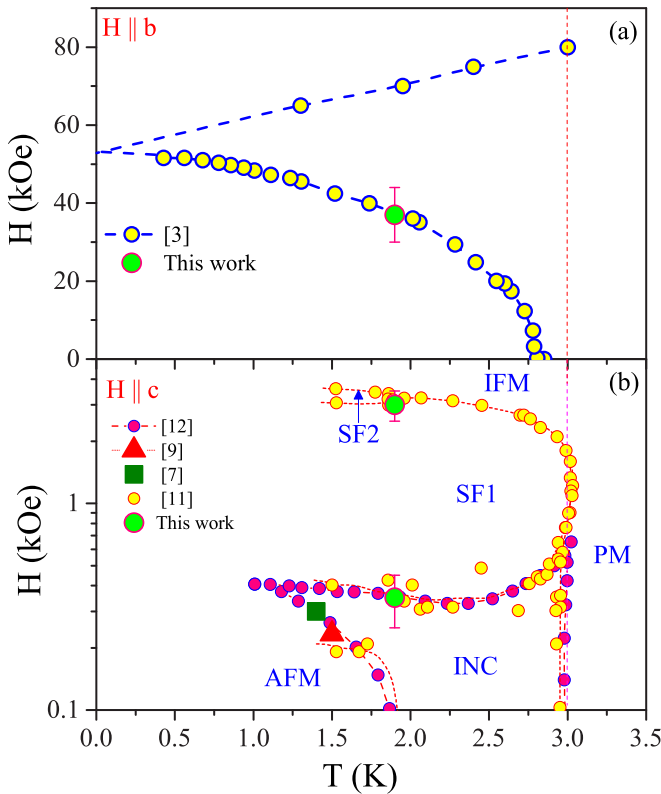


FIG. 1. H - T phase diagram for CoNb_2O_6 for H parallel to the b -axis in (a) and H parallel to the c -axis in (b). Lines connecting the data points are visual guides, and references to sources of the data points are listed in the figure. Green solid circles with error bars are data points from this work based on the peaks in dM/dH vs H shown in Fig. 7(b). The acronyms used for the magnetic phases are as follows: PM, paramagnetic; INC, incommensurate; AFM, antiferromagnetic; SF, spin-flip; and IFM, induced ferromagnetic.

with $T_C = 0$ K for $H_C = 52.5$ kOe [Fig. 1(a)]. For $H > H_C$, effects of quantum spin fluctuations have been reported recently even at nonzero temperatures [2–4]. With an increase in H applied along the c -axis in the IC phase, a spin-flip phase (SF1) is observed for $H_{C1} < H < H_{C2}$, and for $H > H_{C2}$ an induced ferromagnetic (IFM) phase is observed [Fig. 1(b)]. This anisotropic Ising-like linear-chain behavior also became evident from the specific heat data, which showed the presence of significant magnetic entropy well above T_C up to about 25 K [3,9] and broadening and shifting of the peak to higher temperature with an increase in H .

To understand this rich yet complex magnetic phase diagram, good knowledge of the important exchange interactions and anisotropy energies is required. Recent publications by Kobayashi *et al.* [12–14] and Sarvezuk *et al.* [16] have noted that the important exchange interactions among Co^{2+} ions are the intrachain ferromagnetic (FM) exchange constant J_0 along the c -axis and interchain AFM exchange constants J_1 and J_2 in the ab plane using the Hamiltonian

$$H = -J_0 \sum_i S_i^z S_{i+1}^z - J_1 \sum_{i,j} \mathbf{S}_i \cdot \mathbf{S}_j - J_2 \sum_{i,j} \mathbf{S}_i \cdot \mathbf{S}_j, \quad (1)$$

where the sums are over nearest neighbors along the c -axis for J_0 and nearest neighbors and next-nearest neighbors of Co^{2+}

ions, respectively, for J_1 and J_2 in the ab plane. Assuming $S = 3/2$ as the ground state for Co^{2+} ions in CoNb_2O_6 based on Hund's rules, and using the above-listed magnitudes of H_{C1} and H_{C2} and molecular field theory for T_C , Kobayashi *et al.* [12–14] reported that the intrachain ferromagnetic exchange constant $J_0/k_B = 0.6016$ K and it is an order of magnitude larger than the interchain AFM exchange constants $J_1/k_B = -0.0508$ K and $J_2/k_B = -0.0812$ K. Heid *et al.* [11] reported $J_1/k_B = -0.051$ K and $J_2/k_B = -0.029$ K, whereas Sarvezuk *et al.* [16,17] reported $J_0/k_B = 1.18$ K and $J_1/k_B = -0.104$ K.

The focus of this paper is on two issues: (i) The magnitude of effective spin “ S ” of the ground state of Co^{2+} ions in CoNb_2O_6 , $S = 3/2$ as determined by Hund's rules and used in earlier publications [11–17] or $S = 1/2$ as implied or reported in recent papers on CoNb_2O_6 [2–5]; and (ii) redeterminations of the exchange constants since it is argued here that the ground state of Co^{2+} in CoNb_2O_6 has effective $S = 1/2$. Both the effective spin for the ground state of Co^{2+} and accurate values of the intrachain and interchain exchange interactions are important for a proper understanding of the properties of CoNb_2O_6 . The analysis and discussion of the experimental results on the temperature and magnetic field dependence of the magnetization (M) of CoNb_2O_6 presented here show that only $S = 1/2$ (and not $S = 3/2$) can consistently explain the M versus T and M versus H data both above and below T_C . As a result, the new magnitudes of the exchange constants J_0 , J_1 , and J_2 are presented. As discussed in great detail recently in other Co^{2+} containing systems such as $\beta\text{-Co}(\text{OH})_2$ [18], GeCo_2O_4 [19], and CoCl_2 [20], the effective $S = 1/2$ in these systems results from combined effects of noncubic crystalline crystal field and spin-orbit interaction. Details of these results in CoNb_2O_6 along with their discussion and analysis are presented below.

II. MATERIAL SYNTHESIS AND STRUCTURAL CHARACTERIZATION

Bulk polycrystalline samples of CoNb_2O_6 were prepared using the solid-state reaction method starting with stoichiometric proportions of Co_3O_4 and Nb_2O_5 by thoroughly grinding them in an agate mortar/pestle for 5 h, followed by pressing the homogenized powder into pellets of size 15 mm in diameter using a hydraulic press. The pellets were sintered at 1200 °C in air for 8 h. The crystal structure and phase purity of this sintered material were examined using the Rigaku x-ray diffractometer (model: TTRAX III) with $\text{Cu K}\alpha$ ($\lambda = 1.5406$ Å) radiation. The room-temperature x-ray diffraction (XRD) pattern shown in Fig. 2 and refined by the Rietveld technique using the FULLPROF Suite showed that the sample is CoNb_2O_6 without any secondary phases exhibiting an orthorhombic crystal structure [space group $Pbcn-D_{2h}^{14}(no.60)$] with lattice parameters $a = 14.167$ Å, $b = 5.714$ Å, and $c = 5.046$ Å; average bond lengths of 2.025 Å (Co-O) and 1.960 Å (Nb-O); and average bond angles of 106.0° (Nb-O-Nb), 127.8° (Co-O-Nb), and 100.9° (Co-O-Co). The field emission scanning electron micrograph (FESEM) images of CoNb_2O_6 (not shown here) revealed the average size of the grains was ~ 1.7 to 2 μm . The electronic structure and chemical composition of the sample were

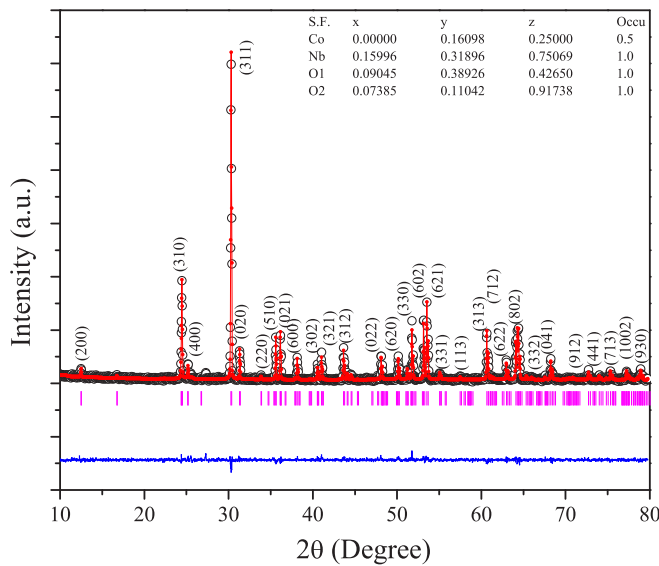


FIG. 2. Room-temperature XRD pattern of the CoNb_2O_6 sample together with the Rietveld refined data and the Miller indices of the Bragg lines listed. The blue line at the bottom represents the difference between the measured and simulated patterns. The inset shows the position of the atoms.

probed using an x-ray photoelectron spectrometer (XPS) from Kratos Analytical (model: AXIS Supra+) configured with a dual monochromatic x-ray source $\text{Al K}\alpha / \text{Ag L}\alpha$ (2984.2 eV) with spatial resolution less than $1 \mu\text{m}$. These XPS spectra (Fig. 3) were calibrated by selecting the binding energy of carbon C 1s orbital (located at $E_C = 284.8 \text{ eV}$) as an internal reference. The O 1s spectrum is resolved into two Gaussian-Lorentzian peaks centered at 528.17 and 529.98 eV. The origin of the most intense peak at 528.17 eV is associated with the bonding between metal and lattice oxygen, whereas the second peak at 529.98 eV is associated with the surface-absorbed oxygen [21–23]. The Nb 3d core level spectrum

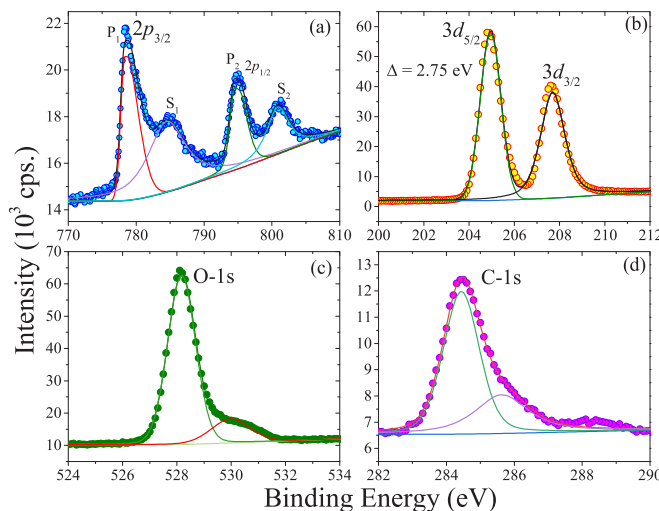


FIG. 3. X-ray photoelectron spectra of (a) Co 2p, (b) Nb 3d, (c) O 1s, and (d) C 1s for the polycrystalline CoNb_2O_6 sample. The solid lines are fits to Gaussian-Lorentzian line shapes.

exhibits two sharp peaks at 204.95 and 207.70 eV with a binding energy separation between these peaks of $\Delta \sim 2.75 \text{ eV}$, which is close to the standard value $\Delta = 2.72 \text{ eV}$, confirming the pentavalent oxidation state of Nb [24]. On the other hand, the deconvolution of the Co 2p core level spectrum consists of four peaks, of which two main peaks (P_1 and P_2) are located at 778.34 and 794.48 eV, respectively, ($2p_{3/2}$ and $2p_{1/2}$). The two broad satellite peaks S_1 and S_2 are centered at 784.51 and 800.87 eV, respectively. The binding energy separation (ΔE) between the doublets P_1 and P_2 (spin-orbit splitting $\Delta E(P_2 - P_1)$) is approximately 16.14 eV, which confirms the divalent oxidation state of Co [19]. The conclusion from the analysis of the XPS data (Fig. 3) shows Co^{2+} and Nb^{5+} as the electronic states in the CoNb_2O_6 sample.

III. MAGNETIC PROPERTIES

A. Temperature and magnetic field dependence of magnetization

The magnetization (M) of the polycrystalline CoNb_2O_6 bulk sample reported here was measured using the vibrating-sample magnetometer (VSM) based physical property measurement system (PPMS-VSM) from Quantum Design (Model: Dynacool) with temperature capabilities from $T = 1.9$ to 400 K in dc-magnetic fields (H) up to $\pm 90 \text{ kOe}$. To measure M versus T , the sample was cooled to 1.9 K in $H = 0$, and a nonzero H was then applied followed by acquiring the data with increasing T after stabilizing the temperature at each T . For M - T measurements, the step size ΔT is 0.02 K, and for M - H measurements the data are recorded at interval $\Delta H = 50$ and 300 Oe for $H < 1500 \text{ Oe}$ and $H > 1500 \text{ Oe}$, respectively.

The temperature dependence of the magnetic susceptibility $\chi = M/H$ for $H = 100 \text{ Oe}$ between $T = 1.9$ and 5 K is shown in Fig. 4(a) with the computed $d\chi/dT$ and $d(\chi T)/dT$ versus T shown in Figs. 4(b) and 4(c), respectively. Usually, a peak in $d\chi/dT$ marks the transition from the PM to the FM state since M versus T data in such cases have an inflection point at T_C [25]. In the PM to AFM transitions at the Néel temperature T_N , it has been shown both theoretically [26] and experimentally [27] that T_N is accurately determined by the peak in $d(\chi T)/dT$ since χT is proportional to magnetic energy near T_N in an antiferromagnet and so the peak in $d(\chi T)/dT$ corresponds to the peak in the specific heat. In the present case, within the resolution of our experiments, peaks in $d\chi/dT$ and $d(\chi T)/dT$ occur at the same temperature, i.e., $T_C = 2.8 \pm 0.1 \text{ K}$ for the PM to the IC state and $T_N = 2.0 \pm 0.1 \text{ K}$ for the IC to the AFM state. These values are close to the magnitude $T_C = 2.85\text{--}2.95 \text{ K}$ and $T_N = 1.97 \text{ K}$ for CoNb_2O_6 reported by others as mentioned in the Introduction. Since our sample is polycrystalline in nature, our data illustrate all the key features of the reported results for H along all three principal directions, although the peaks near T_C and T_N are understandably not as sharp as those observed in single crystals.

The measured data of χ versus T with $H = 300 \text{ Oe}$ and covering the temperature range from 1.9 to 400 K are shown in Fig. 5 with the solid line being a theoretical fit discussed later. We chose $H = 300 \text{ Oe}$ for these measurements up to 400 K since in $H = 100 \text{ Oe}$, the data for $T > 300 \text{ K}$ became

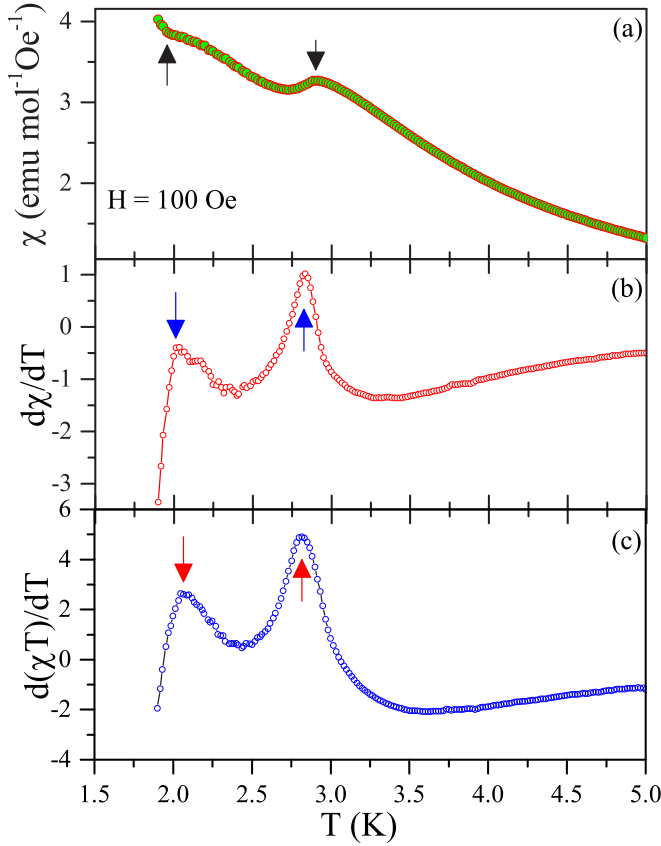


FIG. 4. Plots of $\chi = M/H$ ($H = 100$ Oe) and the computed $d\chi/dT$ and $d(\chi T)/dT$ vs T for the 1.9–5 K range are shown in (a), (b), and (c) respectively. The peaks representing transition points $T_c = 2.0 \pm 0.1$ K and $T_N = 2.8 \pm 0.1$ K are marked by arrows.

noisier due to smaller magnitudes of M at the smaller H . Following the procedures used in the recent papers on several other Co^{2+} containing systems viz. GeCo_2O_4 [19] and Co_2RuO_4 [28], the temperature dependence of paramagnetic susceptibility χ of CoNb_2O_6 for $T > T_c$ was fit to the modified Curie-Weiss (MCW) law given by $\chi = \chi_0 + C/(T - \Theta)$. Here $\chi_0 = \chi_d + \chi_{vv}$ contains contribution from the (negative) diamagnetic susceptibility χ_d and the (positive) van Vleck susceptibility χ_{vv} , both of which have only a very weak temperature dependence [29–31]. All the systems have nonzero χ_d although it may be comparatively negligible [30], whereas χ_{vv} is present in systems with spin-orbit coupling [29,31]. Since χ_d and χ_{vv} are of opposite signs, $\chi_0 = \chi_d + \chi_{vv}$ is often difficult to calculate accurately. Experimentally, χ_0 is determined from the plot of χ versus $1/T$ in the limit of $1/T \rightarrow 0$ with a focus on the high- T data where the contribution from the paramagnetic term $C/(T - \Theta)$ becomes negligible. As shown in Refs. [19,28], the χ_0 term can have a significant effect on the magnitudes of the Curie constant C and Curie-Weiss temperature Θ , the latter expected to be negative (positive) for antiferromagnetic (ferromagnetic) interaction. The fits of the χ versus T data to the CW ($\chi_0 = 0$) and MCW ($\chi_0 = 9.0 \times 10^{-4}$ emu mol $^{-1}$ Oe $^{-1}$) laws, as plots of $(\chi - \chi_0)^{-1}$ versus T , where χ_0 was determined from the plot of χ versus $1/T$ in the limit of $1/T \rightarrow 0$ as shown in the inset of Fig. 6. The slope of the linear fits

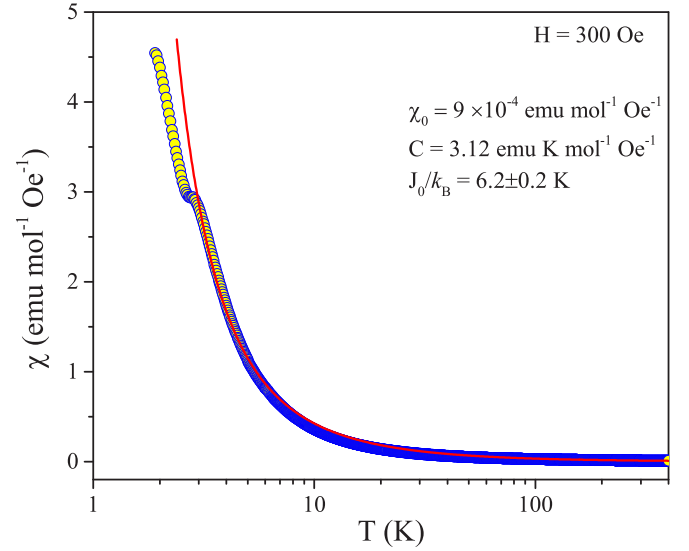


FIG. 5. Temperature dependence of the measured $\chi = M/H$ ($H = 300$ Oe) from 1.9 to 400 K. The solid line is fit to $\chi = \chi_0 + (C/T)\exp(J_0/2k_B T)$ representing the Ising linear chain model with the fitting parameters listed in the figure.

at the higher T yields $1/C$ and intercepts Θ . For $\chi_0 = 0$, the linear fit gives $\Theta = -38$ K, $C = 3.33$ emu K mol $^{-1}$ Oe $^{-1}$, whereas for $\chi_0 = 9 \times 10^{-4}$ emu mol $^{-1}$ Oe $^{-1}$, the linear fit yields positive $\Theta = 11$ K and $C = 3.12$ emu K mol $^{-1}$ Oe $^{-1}$. The negative $\Theta = -38$ K for $\chi_0 = 0$ is not realistic in this case since the dominant exchange interaction is ferromagnetic as noted in earlier publications [2–17] and determined accurately here later. Generally, a negative sign of θ implies that the dominant exchange interaction is antiferromagnetic, whereas in the present case the dominant exchange interaction J_0 between Co^{2+} ions is ferromagnetic, as

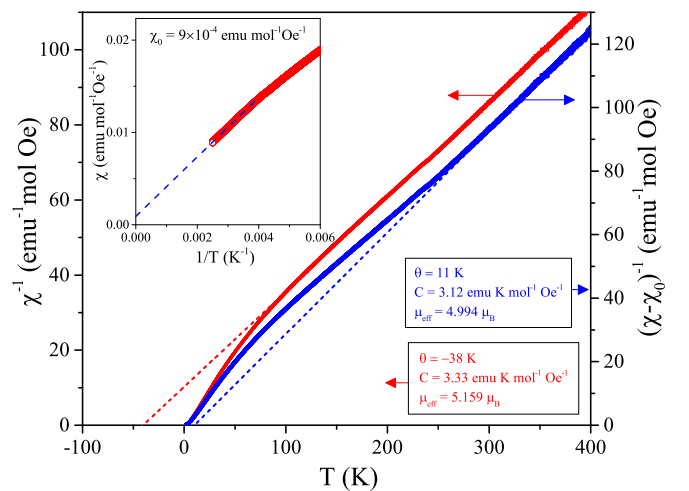


FIG. 6. Plots of $(\chi - \chi_0)^{-1}$ vs T for $\chi_0 = 0$ and 0.0009 emu mol $^{-1}$ Oe $^{-1}$ with the straight line fits for the high-temperature data to determine C and Θ with the numbers given inside the figure and Table I. The inset shows the plot of χ vs $1/T$ to determine χ_0 by linear extrapolation of the high- T data in the limit of $1/T = 0$.

TABLE I. Evaluated and calculated parameters for CoNb_2O_6 using fits to $\chi = \chi_0 + C/(T - \Theta)$ for $\chi_0 = 0$ and $\chi_0 = 0.0009$ ($\text{emu mol}^{-1} \text{Oe}^{-1}$).

Parameters	$\chi_0 = 0.0009$	$\chi_0 = 0$
C ($\text{emu K mol}^{-1} \text{Oe}^{-1}$)	3.12	3.33
μ (CW fit)	$4.994 \mu_B$	$5.159 \mu_B$
Θ	+11K	-38 K
g ($S = 3/2$)	2.579	2.664
g ($S = 1/2$)	5.767	5.957
μ_z ($S = 3/2$)	$3.869 \mu_B$	$3.996 \mu_B$
μ_z ($S = 1/2$)	$2.883 \mu_B$	$2.979 \mu_B$
Calculated M_S (emu mol^{-1})		
($S = 1/2$)	16 101	16 637
($S = 3/2$)	21 608	22 317

discussed later. The magnetic moment μ determined from $C = N_A \mu^2 / 3k_B$ (N_A = Avogadro's constant and k_B = Boltzmann's constant) is $\mu = 5.159 \mu_B$ ($4.994 \mu_B$) for $\chi_0 = 0$ ($\chi_0 = 9 \times 10^{-4} \text{emu mol}^{-1} \text{Oe}^{-1}$). Since $\mu^2 = g^2 S(S+1) \mu_B^2$, these magnitudes of μ are used to calculate g for $S = 1/2$ and $3/2$ and these numbers are given in Table I. It is noted that $g \sim 6$ for Co^{2+} ions in systems with an $S = 1/2$ ground state is quite common [18–20].

The plot of the M versus H data measured at 1.9 K is shown in Fig. 7(a) and that of computed dM/dH versus H is shown in Fig. 7(b) using the log scale for H to highlight the variations for lower H . The peaks in dM/dH versus H are observed at $H_{C1} = 350 \text{Oe}$, $H_{C2} = 3.0 \text{kOe}$, and a broad peak near $H_C = (37 \pm 7) \text{kOe}$. These critical fields, plotted in Fig. 1 with error bars, are in good agreement with earlier measurements performed on single crystals for H parallel to the c - and b -axis, although peaks in our measurements reported here on the polycrystalline sample are understandably diffused. Usually, in the polycrystalline sample, the grains are oriented in different directions, leading to some fraction of grains with their principal axis (a , b , and c) along the applied field. So, in general, one can still expect to observe anomalies such as spin-flip and spin-flop transitions [19], although changes in magnetization associated with the anomalies are expected to be weaker in a polycrystalline sample as compared to those observed in a single crystal in which magnetic field can be oriented along a particular axis. The results plotted in Fig. 1 derived from the peaks in dM/dH versus H shown in Fig. 7(b) are in good agreement with results obtained in single crystals.

B. Effective spin of the magnetic ground state

To distinguish between the $S = 3/2$ and $1/2$ cases as possible ground states for Co^{2+} , the magnitude of the saturation magnetization M_S and magnetic moment μ_z for $T < T_C$ is determined for the two cases and compared with the experimental results, similar to the procedures described in the recent papers on $\beta\text{-Co}(\text{OH})_2$ [18], GeCo_2O_4 [19], and Co_2RuO_4 [28]. Theoretically, $M_S = N_A g S \mu_B$ in the limit of $T = 0 \text{K}$ when all the moments are aligned parallel. Since the magnetic moment of spin S is $g S \mu_B$, this leads to $M_S = N_A g S \mu_B$ per mole when all the moments are aligned parallel yielding the saturation magnetization

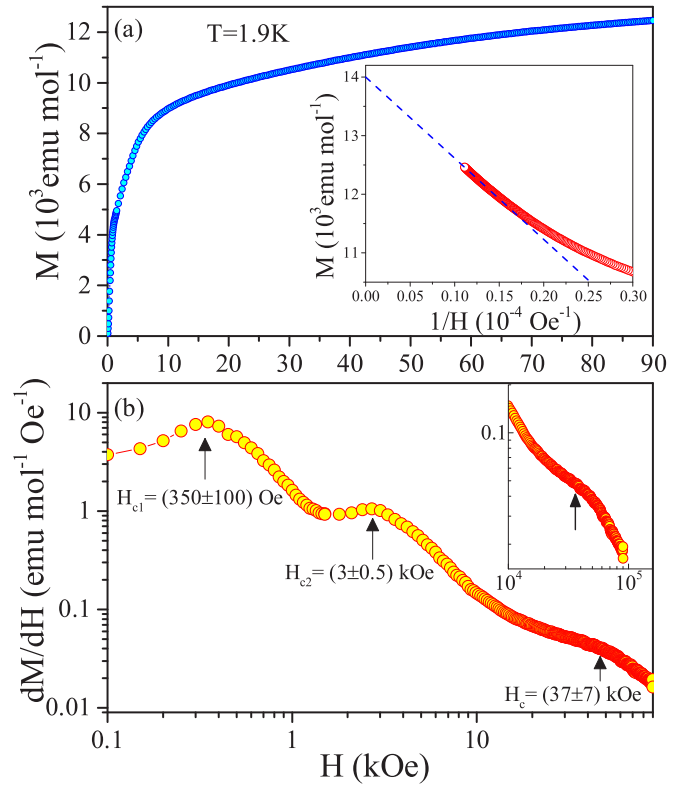


FIG. 7. (a) Plot of the measured magnetization (M) vs applied field H in kOe at 1.9 K. The inset shows a plot of M vs $1/H$ to determine the saturation magnetization M_S by linear extrapolation of the high- H data to $1/H = 0$ shown by the dotted line; (b) plot of computed dM/dH vs H using the data of M vs H in (a). Log scale is used for H to show resolved peaks at low H with the inset showing the broad anomaly centered at 37 kOe. These peak positions marked by arrows are plotted in the H - T phase diagram of Fig. 1.

M_S . Using the magnitudes of g estimated from μ based on the MCW fits for both $S = 1/2$ and $3/2$, the calculated $M_S = 16 101 \text{emu mol}^{-1}$ (by considering $S = 1/2$ and $g = 5.767$) and $M_S = 21 608 \text{emu mol}^{-1}$ (by considering $S = 3/2$ and associated $g = 2.664$) for the case of $\chi_0 = 9 \times 10^{-4} \text{emu mol}^{-1} \text{Oe}^{-1}$. Similar numbers are obtained for $\chi_0 = 0$, which are listed in Table I. Measurements of M_S at 1.8 K for H parallel to the c -axis by Nandi *et al.* [32] yielded $M_S \sim 17 000 \text{emu mol}^{-1}$, which is understandably larger than our experimentally determined $M_S \sim 14 000 \text{emu mol}^{-1}$ at 1.9 K estimated in the inset of Fig. 7(a) since our data are on a polycrystalline sample of CoNb_2O_6 . The important point is that the experimental M_S is closer to the calculated value for the case assuming $S = 1/2$ as the ground state. This is similar to the reported cases of some other Co^{2+} containing systems viz. $\beta\text{-Co}(\text{OH})_2$ [18], GeCo_2O_4 [19], and CoCl_2 [20].

Using neutron diffraction experiments near 1.5 K, Maartense *et al.* [7] and Heid *et al.* [11] reported $\mu/\text{Co}^{2+} = 3.05 \mu_B$ and $3.2 \mu_B$, respectively. Using the above magnitudes of g and S , we have calculated $\mu_z = g S \mu_B = 2.883 \mu_B$ for $S = 1/2$ and $3.869 \mu_B$ for $S = 3/2$ for $\chi_0 = 9 \times 10^{-4} \text{emu mol}^{-1} \text{Oe}^{-1}$, with similar numbers for the $\chi_0 = 0$ case (listed in Table I). This shows again that the experimental results for the measured magnetic moments for $T > T_C$

and $T < T_C$ can be explained only if the ground state of Co^{2+} in CoNb_2O_6 has effective spin $S = 1/2$ and not $3/2$. Interestingly, the agreement between the measured μ_z and M_S for $T < T_C$ and their corresponding calculated values for $S = 1/2$ is somewhat better for the case of $\chi_0 = 0$ than that for $\chi_0 = 9 \times 10^{-4} \text{ emu mol}^{-1} \text{ Oe}^{-1}$ (see Table I). This may be due to the fact that the effect of nonzero χ_0 is only observable for $T > 150 \text{ K}$. The important point is that this reconciliation of the high-temperature and low-temperature magnetic data in CoNb_2O_6 is only possible if the effective spin $S = 1/2$ for the ground state of Co^{2+} . As explained in great detail in [20] with follow-up discussion in [18,19], this effective spin-1/2 state for Co^{2+} results from the combined effects of spin-orbit coupling and noncubic crystalline field. The presence of substantial spin-charge-lattice coupling in CoNb_2O_6 has also been inferred by Nandi *et al.* [32] from their magnetostriction and dielectric constant measurements in CoNb_2O_6 .

C. Exchange constants

Having established $S = 1/2$ as the effective spin for the ground state in CoNb_2O_6 , evaluations of the exchange constants J_0 , J_1 , and J_2 of Eq. (1) are considered next as previous investigators used $S = 3/2$ and $g = 2.1$ in the calculations of J_0 , J_1 , and J_2 [11–13,16] as noted earlier. We first checked and verified the calculations of J_0 , J_1 , and J_2 reported in Ref. [12] using $S = 3/2$ and $g = 2.1$ and then used the same procedure except $S = 1/2$ and $g = 5.767$ were used. For calculation of J_1 and J_2 , the critical fields $H_{C1} = 315 \text{ Oe}$ and $H_{C2} = 3150 \text{ Oe}$ [see Fig. 1(b)] are used along with the tilt angle $\alpha = 31^\circ$. Solving the equations given in [12], the following equations are derived for J_1 and J_2 :

$$J_1 = -g \mu_B \cos\alpha (2H_{C1} + H_{C2}) / (6S), \quad (2)$$

$$J_2 = -g \mu_B \cos\alpha (H_{C2} - H_{C1}) / (6S \cos 2\alpha). \quad (3)$$

These calculations using Eqs. (2) and (3) yield $J_1/k_B = -0.0508 \text{ K}$ and $J_2/k_B = -0.0812 \text{ K}$ obtained for $S = 3/2$ and $g = 2.1$ and reported in Ref. [12]. However, for $S = 1/2$ and $g = 5.767$, $J_1/k_B = -0.42 \text{ K}$ and $J_2/k_B = -0.67 \text{ K}$ are obtained, which are about an order of magnitude larger than values obtained for $S = 3/2$ and the corresponding $g = 2.1$. Similarly, $J_0/k_B = 5.47 \text{ K}$ is obtained using $S = 1/2$ and associated $g = 5.767$ to be compared with $J_0/k_B = 0.6016 \text{ K}$ obtained in Ref. [12] assuming $S = 3/2$ and $g = 2.1$ and the molecular field approximation (MFA) for T_C . These results show that the exchange constants differ by an order of magnitude for the two cases of $S = 1/2$ and $3/2$ along with respective g -values, and so the effective spin $S = 1/2$ established here is also important for an accurate determination of the exchange constants. Using the standard equation for $T_C = J_0 Z S(S+1) / 3k_B$ based on MFA with $Z = 2$ as the number of nearest neighbors for a linear chain and $S = 1/2$ and $T_C = 2.95 \text{ K}$ yields $J_0/k_B = 5.9 \text{ K}$, close to $J_0/k_B = 5.47 \text{ K}$ obtained above.

For a linear ferromagnetic chain with spin $S = 1/2$ and Hamiltonian $H = -J_0 \sum_i S_i^z S_{i+1}^z$, an exact expression for the temperature dependence of magnetic susceptibility χ is avail-

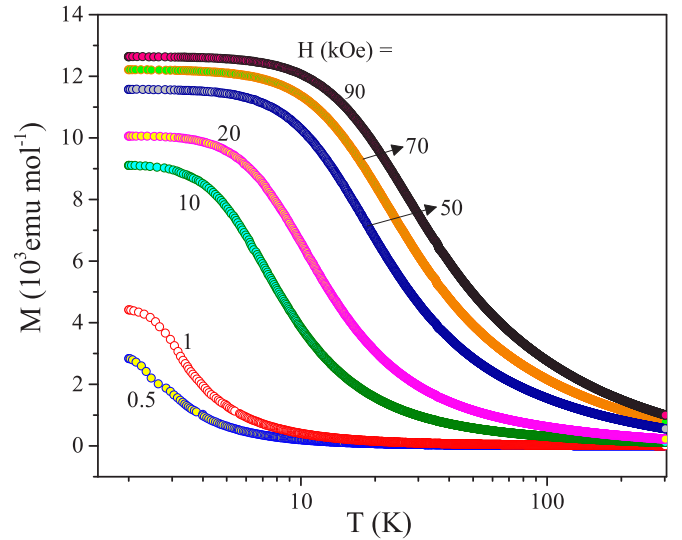


FIG. 8. Temperature dependence of magnetization (M) of CoNb_2O_6 measured in applied $H(\text{kOe}) = 0.5, 1, 10, 20, 50, 70$, and 90 . Log-scale is used for temperature to highlight the variations at lower T .

able [33], and it is given by

$$\chi = \chi_0 + \frac{C}{T} \exp\left(\frac{J_0}{2k_B T}\right). \quad (4)$$

In the above equation, we use $\chi_0 = 0.0009 \text{ emu mol}^{-1} \text{ Oe}^{-1}$ and $C = 3.12 \text{ emu K mol}^{-1} \text{ Oe}^{-1}$ obtained earlier from the fit to MCW law. The best fit of the χ versus T data to Eq. (4), plotted in Fig. 5, shows excellent agreement of the experimental data down to $T_C \sim 3 \text{ K}$ with $J_0/k_B = 6.2 \pm 0.2 \text{ K}$. This magnitude of J_0/k_B , based on the exact expression [Eq. (4)], is only slightly larger than $J_0/k_B = 5.7\text{--}5.9 \text{ K}$ determined earlier based on the MFA.

D. Short-range ordering above T_C

Using a Maxwell equation, the change in the entropy $\Delta S_M = S_M(H) - S_M(0)$ of a material under an applied field H is written as [28]

$$\Delta S_M = \int_0^H \left(\frac{\partial M}{\partial T}\right)_H dH'. \quad (5)$$

In the recent paper on the analysis of M versus T at different H and M versus H at different T in Co_2RuO_4 , the proportionality of $\partial M / \partial T$ to ΔS_M in terms of their temperature variations was demonstrated [28]. In Co_2NbO_6 , we have used this proportionality to determine ΔS_M from the M versus T data at different H . The plots of M versus T in the presence of different external fields up to 90 kOe are shown in Fig. 8 and the computed $(-\partial M / \partial T)$ versus T for different H are shown in Fig. 9. Since the applied magnetic field in PM and FM systems improves magnetic ordering and hence lowers the entropy, ΔS_M and hence $\partial M / \partial T$ are negative. For the lowest $H = 0.5 \text{ kOe}$, $(-\partial M / \partial T)$ versus H shows two peaks, one at $T_N = 2.0 \text{ K}$ and the second near $T_C = 3.0 \text{ K}$. For $H = 1 \text{ kOe}$, only a single peak near $T_C = 3.0 \text{ K}$ is observed, which, with an increase in H , becomes broader and shifts to higher T ; this shift quantified in the plot is shown in the

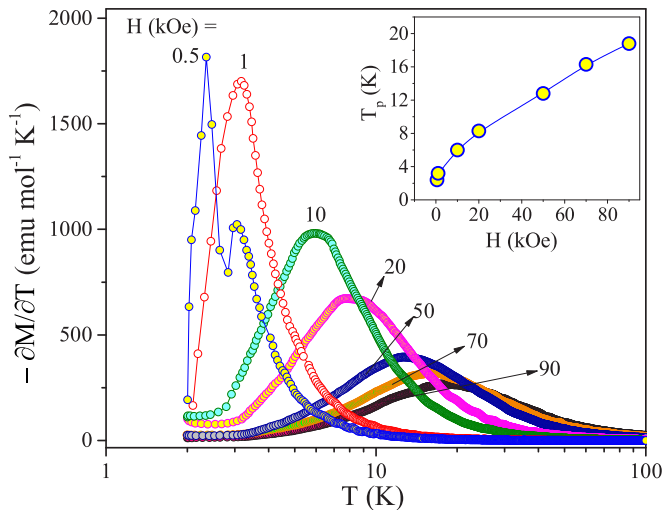


FIG. 9. Plots of the computed $(-\partial M/\partial T)$ vs temperature for different H (marked by arrows) using the data of M vs T of Fig. 8. The very weak oscillations in some curves are artefacts of the numerical computation of $\partial M/\partial T$ from the M vs T data, whereas the magnetic field dependence of the broader peak position T_p of $(-\partial M/\partial T)$ vs H is shown in the inset, with the line connecting the data points as a visual guide.

inset of Fig. 9. This H -dependence of the peak is very similar to the observation of the H -dependence of the peak in the specific heat versus temperature data reported for CoNb_2O_6 in [3,9], thus providing a semiquantitative correlation between the specific heat and magnetization data. These observations point to a significant amount of short-range magnetic ordering well above T_C in this pseudo-one-dimensional Ising system, which is enhanced by the applied field. This effective increase of T_C with an increase in magnetic field in a ferromagnet has been explained in a recent report [25] in terms of the coupling and enhancement of the order parameter (magnetization) of a ferromagnet with applied field.

IV. CONCLUDING REMARKS

Analysis of the M versus T and M versus H data in CoNb_2O_6 presented here leads to the conclusion that the

effective spin for the ground state of Co^{2+} is $S = 1/2$ and not $S = 3/2$ usually expected from Hund's rules and assumed in some earlier publications. The effective spin $S = 1/2$ of the ground state in CoNb_2O_6 results from the combined effects of a noncubic crystalline field, and spin-orbit coupling is also reported in some other Co^{2+} containing systems [18–20]. Using $S = 1/2$ and the associated $g = 5.767$ for the ground state in CoNb_2O_6 , the exchange constants $J_0/k_B = 6.2$ K, $J_1/k_B = -0.42$ K, and $J_2/k_B = -0.67$ K are determined where the intrachain J_0 is ferromagnetic in nature and it is an order of magnitude larger than the interchain antiferromagnetic exchange constants J_1 and J_2 .

The excellent fit of the temperature dependence of paramagnetic susceptibility of CoNb_2O_6 to the Ising linear chain model with $J_0/k_B = 6.2$ K in Fig. 5 shows that magnetic anisotropy along the chain c -axis is much larger than the magnetic anisotropy in the ab plane. The critical field $H_C = 52.5$ kOe applied along the b -axis for which T_C is forced to 0 K (Fig. 1) is effectively equal to $J_0/k_B = 6.2$ K in temperature units ($1 \text{ K} \sim 10 \text{ kOe}$) and it provides a measure of the Ising anisotropy of the system. However, a theoretical interpretation of the experimental variation of T_C versus H for H along the b -axis (shown in Fig. 1) has not yet been reported. Also the accurate magnitude of the weaker anisotropy in the ab plane needs to be determined. Therefore, additional experimental and theoretical investigations of these issues in this interesting system are warranted.

ACKNOWLEDGMENTS

S.T. acknowledges the FIST programme of Department of Science and Technology, India for partial support of this work (Refs. No. SR/FST/PSII-020/2009 and No. SR/FST/PSII-037/2016). R.M. and R.S.R. would like to acknowledge the Ministry of Education (MOE), Singapore through Grant No. MOE2019-T2-1-058 and National Research Foundation (NRF) through Grant No. NRF-CRP21-2018-003. S.T. acknowledge Dr. Sobhit Singh (from Rutgers, The State University of New Jersey), for his helpful discussions. M.R. acknowledge the financial support from University Grants Commission (UGC), Ministry of Education (MOE), Government of India.

-
- [1] S. Sachdev, *Quantum Phase Transition* (Cambridge University Press, Cambridge, 1999).
 - [2] R. Coldea, D. A. Tennant, E. M. Wheeler, E. Wawrzynska, D. Prabhakaran, M. Telling, K. Habicht, P. Smeibidl, and K. Kiefer, *Science* **327**, 177 (2010).
 - [3] T. Liang, S. M. Koohpayeh, J. W. Krizan, T. M. McQueen, R. J. Cava, and N. P. Ong, *Nat. Commun.* **6**, 7611 (2015).
 - [4] A. W. Kinross, M. Fu, T. J. Munsie, H. A. Dabkowska, G. M. Luke, S. Sachdev, and T. Imai, *Phys. Rev. X* **4**, 031008 (2014).
 - [5] C. M. Morris, R. Valdes-Anguilera, A. Ghosh, S. M. Koohpayeh, J. Krizan, R. J. Cava, O. Tchernyshyov, T. M. McQueen, and N. P. Armitage, *Phys. Rev. Lett.* **112**, 137403 (2014).
 - [6] H. Weitzel and S. Klein, *Solid State Commun.* **12**, 113 (1973).
 - [7] I. Maartense, I. Yaeger, and B. M. Wanklyn, *Solid State Commun.* **21**, 93 (1977).
 - [8] W. Scharf, H. Weitzel, I. Yaeger, I. Maartense, and B. M. Wanklyn, *J. Magn. Mater.* **13**, 121 (1979).
 - [9] T. Hanawa, K. Shinkawa, M. Ishikawa, K. Miyatani, K. Saito, and K. Kohn, *J. Phys. Soc. Jpn.* **63**, 2706 (1994).
 - [10] S. Mitsuda, K. Hosoya, T. Wada, H. Yoshizawa, T. Hanawa, M. Ishikawa, K. Miyatani, K. Saito, and K. Kohn, *J. Phys. Soc. Jpn.* **63**, 3568 (1994).
 - [11] C. Heid, H. Weitzel, P. Burlet, M. Bonnet, W. Gonschorek, T. Vogt, J. Norwig, and H. Fuess, *J. Magn. Mater.* **151**, 123 (1995).
 - [12] S. Kobayashi, S. Mitsuda, M. Ishikawa, K. Miyatani, and K. Kohn, *Phys. Rev. B* **60**, 3331 (1999).

- [13] S. Kobayashi, S. Mitsuda, and K. Prokes, *Phys. Rev. B* **63**, 024415 (2000).
- [14] S. Kobayashi, H. Okano, T. Jogetsu, J. Miyamoto, and S. Mitsuda, *Phys. Rev. B* **69**, 144430 (2004).
- [15] S. Kobayashi, S. Mitsuda, S. Hosaka, H. Tamatsukuri, T. Nakajima, H. Koorikawa, K. Prokeš, and K. Kiefer, *Phys. Rev. B* **94**, 134427 (2016).
- [16] P. W. C. Sarvezuk, E. J. Kinast, C. V. Colin, M. A. Gusmao, J. B. M. da Cunha, and O. Isnard, *Phys. Rev. B* **83**, 174412 (2011).
- [17] P. W. C. Sarvezuk, E. J. Kinast, C. V. Colin, M. A. Gusmão, J. B. M. da Cunha, and O. Isnard, *J. Appl. Phys.* **109**, 07E160 (2011).
- [18] Z. Wang and M. S. Seehra, *J. Phys.: Condens. Matter.* **29**, 225803 (2017).
- [19] P. Pramanik, S. Ghosh, P. Yanda, D. C. Joshi, S. Pittala, A. Sundaresan, P. K. Mishra, S. Thota, and M. S. Seehra, *Phys. Rev. B* **99**, 134422 (2019).
- [20] M. E. Lines, *Phys. Rev.* **131**, 546 (1963).
- [21] N. McIntyre and D. Zetaruk, *Anal. Chem.* **49**, 1521 (1977).
- [22] T.-H. Ko, K. Devarayan, M.-K. Seo, H.-Y. Kim, and B.-S. Kim, *Sci. Rep.* **6**, 20313 (2016).
- [23] H. Nesbitt and D. Banerjee, *Am. Mineral.* **83**, 305 (1998).
- [24] J. Geyer-Lippmann, A. Simon, and F. Z. Stollmaier, *Anorg. Allg. Chem.* **516**, 55 (1984).
- [25] N. Mottaghi, M. S. Seehra, J. Shi, M. Jain, and M. B. Holcomb, *J. Appl. Phys.* **128**, 073903 (2020).
- [26] M. E. Fisher, *Philos. Mag.* **7**, 1731 (1962).
- [27] E. E. Bragg and M. S. Seehra, *Phys. Rev. B* **7**, 4197 (1973).
- [28] S. Ghosh, D. C. Joshi, P. Pramanik, S. K. Jena, S. Pittala, T. Sarkar, M. S. Seehra, and S. Thota, *J. Phys.: Condens. Matter* **32**, 485806 (2020).
- [29] N. D. Mermin and N. W. Ashcroft, *Solid State Physics* (Holt, Rinehart and Winston, New York, 1976), pp 644–653.
- [30] L. B. Mendelsohn, F. Biggs, and J. B. Mann, *Phys. Rev. A* **2**, 1130 (1970).
- [31] P. Burgardt and M. S. Seehra, *Solid State Commun.* **22**, 153 (1977).
- [32] M. Nandi, D. Prabhakaran, and P. Mandal, *J. Phys.: Condens. Matter* **31**, 195802 (2019).
- [33] C. Coulon, H. Miyasaka, and R. Clerac, *Struct. Bond* **122**, 163 (2006).